

DYNAMICAL CUSP REGENERATION

DAVID MERRITT AND ANDRAS SZELL

Department of Physics, Rochester Institute of Technology, Rochester, NY 14623

Draft version 13th November 2018

Abstract

After being destroyed by a binary supermassive black hole, a stellar density cusp can regrow at the center of a galaxy via energy exchange between stars moving in the gravitational field of the single, coalesced hole. We illustrate this process via high-accuracy N -body simulations. Regeneration requires roughly one relaxation time and the new cusp extends to a distance of roughly one-fifth the black hole's influence radius, with density $\rho \sim r^{-7/4}$; the mass in the cusp is of order 10% the mass of the black hole. Growth of the cusp is preceded by a stage in which the stellar velocity dispersion evolves toward isotropy and away from the tangentially-anisotropic state induced by the binary. We show that density profiles similar to those observed at the center of the Milky Way and M32 can regenerate themselves in several Gyr following infall of a second black hole; the presence of density cusps at the centers of these galaxies can therefore not be used to infer that no merger has occurred. We argue that $\rho \sim r^{-7/4}$ density cusps are ubiquitous in stellar spheroids fainter than $M_V \approx -18.5$ that contain supermassive black holes, but the cusps have not been detected outside of the Local Group since their angular sizes are less than $\sim 0.1''$. We show that the presence of a cusp implies a lower limit of $\sim 10^{-4} \text{ yr}^{-1}$ on the rate of stellar tidal disruptions, and discuss the consequences of the cusps for gravitational lensing and the distribution of dark matter on sub-parsec scales.

Subject headings:

1. INTRODUCTION

Mass distributions near the centers of early-type galaxies are well described as power laws, $\rho \sim r^{-\gamma}$, with indices γ that change gradually with radius. At their innermost resolved radii, most galaxies have $0.5 \lesssim \gamma \lesssim 2.$, with the steeper slopes characteristic of fainter galaxies (Ferrarese et al. 2005). If a supermassive black hole is present, the orbits of stars will be strongly influenced at distances less than $\sim r_h = GM_\bullet/\sigma^2 \approx 10 \text{ pc } (M_\bullet/10^8 M_\odot)(\sigma/200 \text{ km s}^{-1})^{-2}$, the black hole's gravitational influence radius. Most galaxies are spatially unresolved on these small scales; two clear exceptions are the nucleus of the Milky Way, for which number counts extend inward to $\sim 0.002 r_h$ (Genzel et al. 2003), and M32, which is resolved down to a radius of $\sim 0.2 r_h$ (Lauer et al. 1998). Both galaxies exhibit steep density slopes, $\gamma \approx 1.5$, at $r \lesssim r_h$. Outside of the Local Group, only giant ellipticals have sufficiently large black holes that r_h can be resolved; the nuclear luminosity profiles in these galaxies are also power laws but very flat, $\gamma \lesssim 1$.

Many distributions of stars are possible around a black hole, but under two circumstances, the stellar distribution at $r \lesssim r_h$ is predictable. (1) If the black hole has been present for a time longer than T_r , the relaxation time in the nucleus, exchange of energy between stars will drive the stellar distribution toward a collisional steady state; assuming a single stellar mass and ignoring physical collisions between stars, this steady state has $\rho \sim r^{-7/4}$ at $r \lesssim r_h$ (Bahcall & Wolf 1976). (2) If the nucleus formed via the merger of two galaxies each with its own supermassive black hole, the two black holes will displace of order their combined mass in the process of forming a tightly-bound pair (Milosavljevic & Merritt 2001), producing a low-density core. The first mechanism may be responsible for the steep density profiles observed at the centers of the Milky Way and M32, since both galaxies have central relaxation times of order 10^9 yr and both are near enough that linear scales of order r_h are well re-

solved. The second mechanism may explain the very flat central profiles of luminous E galaxies (Milosavljevic et al. 2002; Ravindranath, Ho & Filippenko 2002); the central relaxation times of these galaxies are much longer than 10^{10} yr and the stellar distribution would be expected to remain nearly unchanged after the two black holes had coalesced into one.

In this paper we point out that both outcomes are possible. A galaxy may form via mergers, but at the same time, its central relaxation time following the merger may be shorter than 10^{10} yr . In this circumstance, the cusp of stars around the black hole is first destroyed by the massive binary, then is regenerated via encounters between stars in the gravitational field of the single, coalesced hole. The result is a steep inner density profile in a galaxy that had previously experienced the scouring effects of a massive binary. To the extent that *all* stellar spheroids experienced mergers – if only in the distant past – this picture is probably generic, applying even to small dense systems like M32 and to the bulges of spiral galaxies like the Milky Way. Understanding the conditions under which a previously-destroyed density cusp can spontaneously regenerate is crucial if one wishes to interpret the present-day luminosity profiles of galaxies as fossil relics of their merger histories (Volonteri et al. 2003).

We use N -body simulations (§2) to follow first the destruction (§3) and then the spontaneous regeneration (§4) of density cusps around black holes. The two most important free parameters in this problem are the mass ratio $q \equiv M_2/M_1$ of the binary black hole, and the slope γ of the initial density cusp surrounding the larger hole. We present results for several combinations of q and γ (Table 1). Our conclusion is that collisional, Bahcall-Wolf density cusps should be ubiquitous in stellar spheroids fainter than $M_V \approx -18.5$ that contain massive black holes, essentially regardless of their merger histories. However these cusps have gone undetected in galaxies outside the Local Group because they are unresolved. In §5 we discuss a number of consequences of the presence of the cusps.

TABLE 1
PARAMETERS OF THE N -BODY INTEGRATIONS

Run	γ	M_2/M_1	r_{h1}	r_{h12}	$T_r(r_{h12})$	a_h	r'_h	$T_r(r'_h)$	$T_r(0.2r'_h)$	T_{gap}	r''_h
1	0.5	0.5	0.264	0.326	1170.	0.0181	0.39	1420.	620	79.	0.38
2	0.5	0.25	0.264	0.296	1010.	0.0119	0.35	1210.	420	48.	0.34
3	0.5	0.1	0.264	0.278	916.	0.00573	0.32	1070.	390	22.	0.31
4	1.0	0.5	0.165	0.210	599.	0.0116	0.28	870.	300	48.	0.27
5	1.0	0.25	0.165	0.188	499.	0.00751	0.23	640.	270	26.	0.23
6	1.0	0.1	0.165	0.174	441.	0.00360	0.20	520.	220	11.	0.20
7	1.5	0.5	0.0795	0.107	217.	0.00594	0.17	420.	160	23.	0.17
8	1.5	0.25	0.0795	0.093	170.	0.00364	0.13	260.	110	10.	0.13
9	1.5	0.1	0.0795	0.085	144.	0.00176	0.11	200.	75	4.1	0.11

2. MODELS AND METHODS

We started by constructing Monte-Carlo realizations of steady-state galaxy models having Dehnen’s (1993) density law, with an additional, central point mass representing a black hole. The Dehnen-model density follows $\rho(r) \propto r^{-\gamma}$ at small radii, and the isotropic phase-space distribution function that reproduces Dehnen’s $\rho(r)$ in the presence of a central point mass is non-negative for all $\gamma \geq 0.5$; hence $\gamma = 0.5$ is the flattest central profile that can be adopted if the initial conditions are to represent an isotropic, steady state. We considered initial models with $\gamma = (0.5, 1.0, 1.5)$. The mass M_1 of the central “black hole” was always 0.01, in units where the total mass in stars M_{gal} was one; the Dehnen scale length r_D and the gravitational constant G were also unity. The N -body models so constructed were in a precise steady state at time zero.

Destruction of the cusp was achieved by introducing a second “black hole” into this model, which spiralled into the center, forming a binary with the first (more massive) hole and displacing stars. Three values were used for the mass of the smaller hole: $M_2/M_1 \equiv q = (0.5, 0.25, 0.1)$. The smaller hole was placed initially at a distance 1.6 from the center, with a velocity roughly $1/2$ times the circular velocity at that radius; a non-circular orbit was chosen in order to speed up the orbital decay.

After the orbit of the smaller black hole had decayed via dynamical friction against the stars, it formed a tight binary with the more massive hole, with a relative orbit close to circular. An estimate of the semi-major axis a_h at which the binary first becomes “hard” is $a_h = G\mu/4\sigma^2$ where $\mu \equiv M_1M_2/(M_1 + M_2)$ is the reduced mass. The precise meaning of “hard” is debatable; the definition just given defines a “hard” binary as one whose binding energy per unit mass, $|E|/(M_1 + M_2)$, exceeds $2\sigma^2$. While simple, this definition contains the ill-defined quantity σ , which is a steep function of position near the black hole(s). We followed Merritt & Wang (2005) and used the alternative definition

$$a_h \equiv \frac{\mu}{M_1 + M_2} \frac{r_{h12}}{4} = \frac{q}{(1+q)^2} \frac{r_{h12}}{4}, \quad (1)$$

with r_{h12} the gravitational influence radius defined below. In practice, a_h so defined was found to be roughly (within a factor ~ 2) the value of the semi-major axis at which the binary hardening rate $(d/dt)(1/a)$ first became approximately constant.

Decay was allowed to continue until the binary semi-major axis had reached a value of $a_h/5 \approx qr_h/20$. At this point,

the two black holes were replaced by a single particle of mass $M_{12} = M_1 + M_2$, with position and velocity given by the center of mass of the binary. The N -body integration was then continued for a time roughly equal to the relaxation time $T_r(r'_h)$ defined below. The most suitable time at which to merge the two black holes was not clear *a priori*; our choice is of order the separation at which gravitational-wave emission would induce coalescence in $\sim 10^{10}$ yr (Merritt & Milosavljevic 2005), but in fact we expect that other processes like interaction of the binary with ambient gas may drive the final coalescence in real galaxies, and it is not clear at what separation these processes are likely to dominate the evolution.

The ratio $(M_1 + M_2)/M_{gal} \approx 0.01$ in our models is roughly a factor ten larger than the ratio of black hole mass to galaxy mass in real spheroids (Merritt & Ferrarese 2001; Marconi & Hunt 2003). This is acceptable as long as we are careful to present masses and radii in units scaled to $M_1 + M_2$ when making comparisons with real galaxies.

Table 1 gives a number of parameters associated with the N -body integrations. The gravitational influence radius r_h was defined as the radius containing a mass in stars equal to twice the mass M_\bullet of the central black hole. This definition, while superior to GM_\bullet/σ^2 , is somewhat ambiguous in our N -body models, given that the effective mass of the central object, and the distribution of the stars, both change with time. We accordingly defined four different influence radii. (1) At the start of the integrations, the larger black hole, of mass M_1 , was located at the center of the galaxy. Its influence radius r_{h1} was computed by setting $M_\bullet = M_1$ and using the $t = 0$ stellar distribution. (2) After the smaller black hole has fallen in to a distance $\lesssim r_{h1}$ from the larger hole, the appropriate value of M_\bullet becomes $M_1 + M_2$. We defined the associated influence radius to be r_{h12} , which we computed ignoring the changes that had occurred in the stellar distribution since $t = 0$. (3) The third influence radius, r'_h , was computed by setting $M_\bullet = M_1 + M_2$, but this mass was compared with the stellar distribution at the end of the binary evolution phase, after the phase of cusp destruction. (4) Finally, r''_h is the influence radius at the end of the second phase of integration, after a Bahcall-Wolf cusp has formed around the single black hole. As Table 1 shows, r''_h is only slightly smaller than r'_h since the regenerated cusp contains a mass that is small compared with M_\bullet .

The relaxation times T_r in Table 1 were computed from the standard expression (eq. 2-62 of Spitzer 1987), setting $\ln \Lambda = \ln(\sigma^2 r_{h12}/2Gm_\star)$, with σ the 1D stellar velocity dispersion at r_{h12} and $m_\star = N^{-1}$ the mass of an N -body particle.

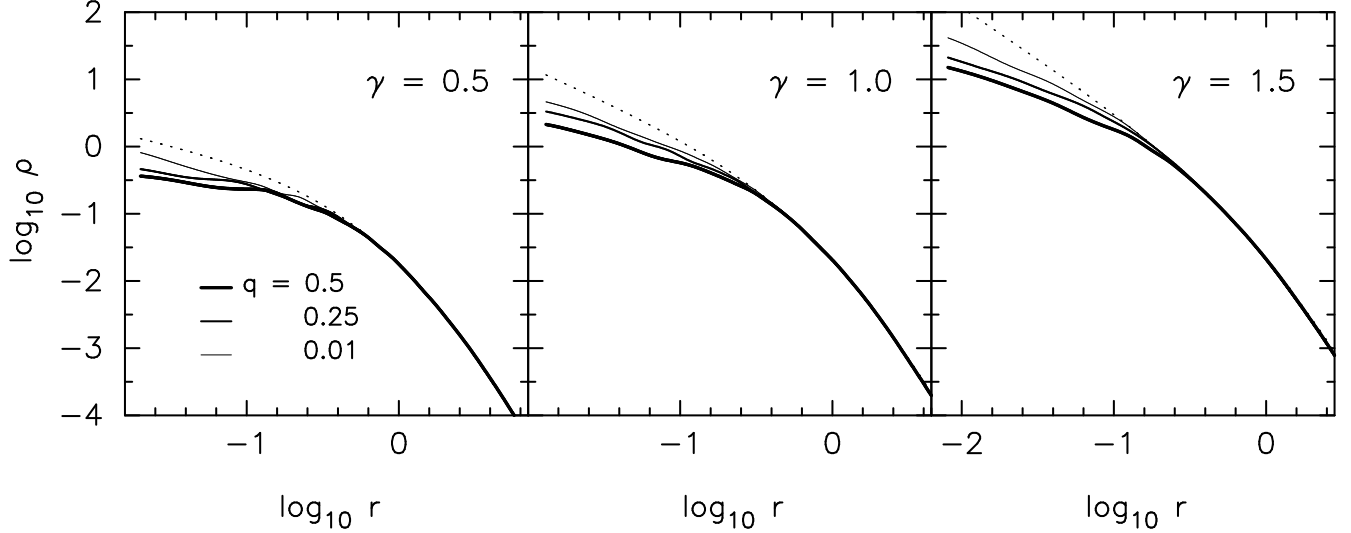


FIG. 1.— Cusp destruction. Solid lines are stellar density profiles just before the two “black holes” were combined into one. Dashed lines show the initial models. $q = M_2/M_1$ is the binary mass ratio.

This definition of Λ is equivalent to equating b_{max} , the maximum impact parameter for encounters in Chandrasekhar’s theory, with r_h (Preto, Merritt & Spurzem 2004). Table 1 gives values of T_r evaluated at two of the four influence radii defined above. $T(r_{h12})$ was computed using the structural parameters of the initial galaxy model, while $T_r(r'_h)$ was computed using estimates like those in Figures 1 and 3. of the stellar density and velocity dispersion in the evolved models. We also give $T_r(0.2rh')$; the motivation for this is given below. The final time scale in Table 1, T_{gap} , is defined below (equation 7) and is an estimate of the time required for the angular-momentum gap created by the binary to be refilled; T_{gap} varied between $\sim T_r(r_h)/20$ and $\sim T_r(r_h)/50$.

The power-law cusps in our initial models were motivated by the approximately power-law dependence of luminosity density on radius observed near the centers of many early-type galaxies (Ferrarese et al. 2005). Since the observations often do not resolve r_h , the stellar distribution at $r \lesssim r_h$ in some galaxies might be different than the inward extrapolation of the power laws that are fit to larger radii. For instance, galaxies with sufficiently short relaxation times are expected to have $\rho \sim r^{-7/4}$ density cusps like the ones that form in our N -body models at late times. Other galaxies may have compact stellar nuclei (Coté et al. 2005). We did not include such dense features in our initial models: first, because the associated mass would have been small compared with the mass removed by the binary; and second, because doing so would have more than doubled the computational effort due to the short time steps required for stars initially near the black holes.

All N -body integrations used $N = 0.12 \times 10^6$ particles and were carried out on a GRAPE-6 special-purpose computer. The N -body integrator is described in Merritt, Mikkola & Szell (2006). This algorithm is an adaptation of NBODY1 Aarseth (1999) to the GRAPE-6; it uses a fourth-order Hermite integration scheme with individual, adaptive, block time steps (Aarseth 2003). For the majority of the particles, the forces and force derivatives were calculated via a direct-summation scheme on the GRAPE-6, using the particle advancement scheme described

in Berczik, Merritt & Spurzem (2005) with an accuracy parameter of $\eta = 0.01$ and zero softening. Close encounters between the black holes, and between black holes and stars, require prohibitively small time steps in such a scheme and were regularized using the chain regularization routine of Mikkola and Aarseth (Mikkola & Aarseth 1990, 1993). A detailed description of the chain algorithm, including the results of performance tests, are given in Merritt, Mikkola & Szell (2006).

Our initial conditions (one black hole at the center, a smaller black hole orbiting about it) are not as realistic as in simulations that follow both merging galaxies from the start (e.g. Milosavljevic & Merritt (2001), Merritt et al. (2002)), but are superior to simulations that drop one or two black holes into a pre-existing galaxy that contains no black hole (e.g. Quinlan & Hernquist (1997); Nakano & Makino (1999a,b)). We ignore the radiation recoil that would accompany the final coalescence of the two black holes, displacing the remnant hole temporarily from its central location and increasing the size of the core (Merritt et al. 2004b; Boylan-Kolchin et al. 2004). We also ignore processes like loss of stars into the black hole(s), stellar tidal disruptions, and stellar collisions, all of which might affect the form of the final density profile.

3. CUSP DESTRUCTION

After formation of a hard binary at $a \approx a_h$, the binary’s binding energy continues to increase as the two massive particles eject stars via the gravitational slingshot (Saslaw, Valtonen & Aarseth 1974; Mikkola & Valtonen 1992; Quinlan 1996). As in a number of recent studies (Berczik, Merritt & Spurzem 2005; Merritt, Mikkola & Szell 2006), we found that the hardening rates were nearly independent of time, $s \equiv (d/dt)(1/a) \approx \text{const.}$, for $a < a_h$. The values of s are not of particular interest here, since N -body hardening rates are known to depend strongly on particle number (Berczik, Merritt & Spurzem 2005), and we do not expect these simulations to be in the “empty loss cone” regime that characterizes binary evolution in real galaxies (Milosavljevic & Merritt 2003). However the “damage” done by the binary to the pre-existing stellar distribution is expected on energetic grounds to be a function of a_h/a , essentially independent of the *rate* of hardening and hence of N (Quinlan

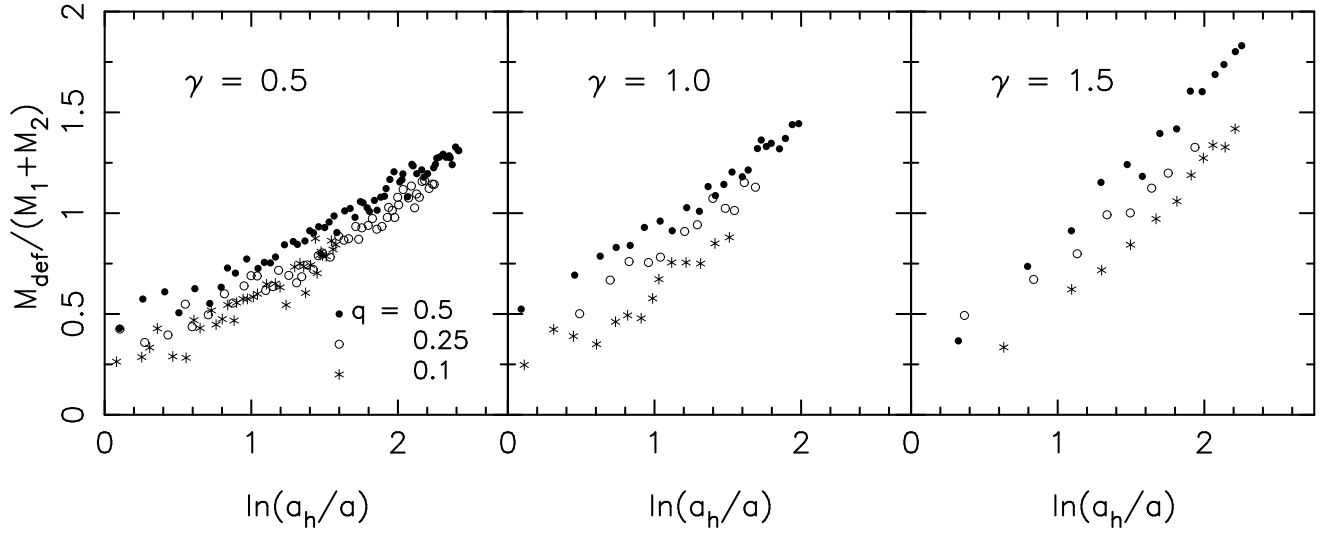


FIG. 2.— Mass deficits, computed as described in the text, during the binary phase of the integrations; $a = a(t)$ is the binary semi-major axis and a_h is defined in equation (1). $q = M_2/M_1$ is the binary mass ratio.

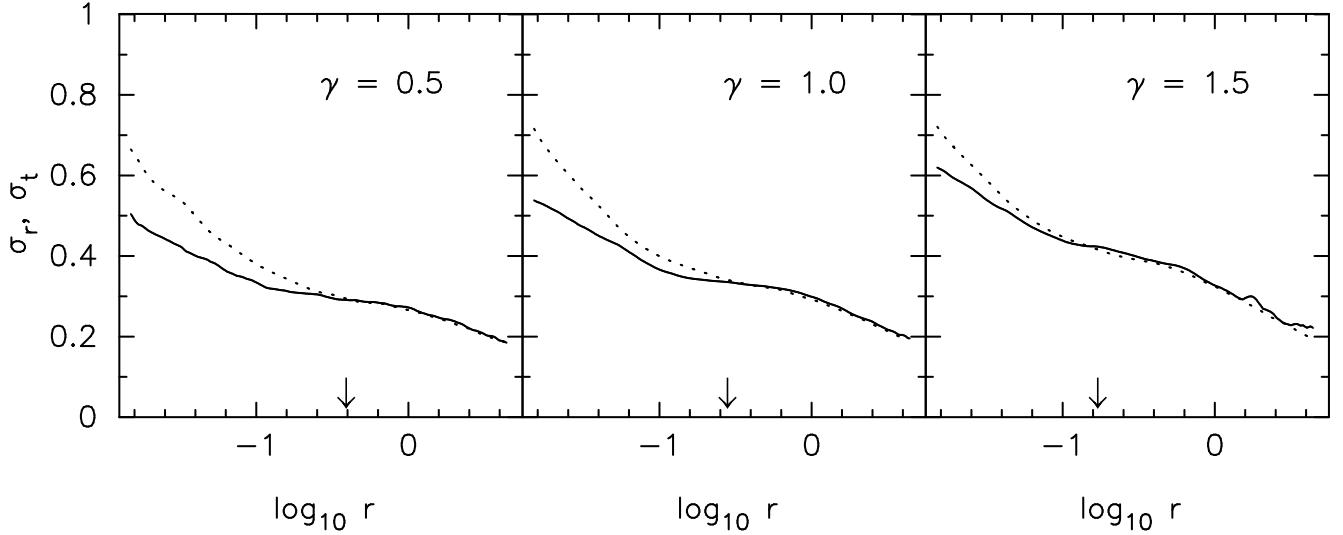


FIG. 3.— Stellar velocity dispersions at the end of the binary phase, in the integrations with $M_2/M_1 = 0.5$. Solid lines: σ_r ; dashed lines: σ_t . The binary creates a tangentially-biased velocity distribution near the center by preferentially ejecting stars on radial orbits. Arrows indicate the black hole influence radius r'_h .

1996), and this expectation has recently been confirmed in N -body experiments (Merritt, Mikkola & Szell 2006). As described above, the binary phase of the integrations was terminated when $a = a_h/5$.

Figure 1 shows density profiles of the N -body models at the end of the binary phase. Radii of the “star” particles were computed relative to the center of mass of the binary, and estimates of $\rho(r)$ were constructed using the nonparametric kernel estimator of Merritt & Tremblay (1994). The damage done by the infalling black hole can be seen to increase with its mass for $\gamma = 0.5$ and 1, and extends out to a radius $\sim r_h$. The $\gamma = 0.5$ cusp is converted into an approximately constant-density core, while the $\gamma = 1$ and $\gamma = 1.5$ cusps are “softened,” to power laws of index ~ 0.5 ($\gamma = 1$) and ~ 1.0 ($\gamma = 1.5$).

A standard measure of the damage done by an infalling black hole to a pre-existing density cusp is the “mass deficit” M_{def} , defined as the decrease in the central mass within a sphere that contains the affected region (Milosavljevic et al. 2002). The mass deficit is potentially observable

(Milosavljevic et al. 2002; Ravindranath, Ho & Filippenko 2002; Graham 2004), assuming that one can guess the pre-existing density profile, and its value is an index of the cumulative effect of mergers on the galaxy (Volonteri et al. 2003). Since there are few results in the literature on the sizes of mass deficits generated by large-mass-ratio inspirals, we show in Figure 2 mass deficits for these integrations, expressed in terms of $a_h/a(t)$; we extended some of the integrations beyond $a = a_h/5$ in order to further elucidate this dependence. Figure 2 shows that – for a given degree of binary hardness – the mass deficit is much better predicted by M_1 or M_{12} than by M_2 . In other words, the damage done by the smaller black hole is roughly proportional to the mass of the *binary*, at a given value of a_h/a .

This is a reasonable result. Equating the increase in the binary’s binding energy with the energy lost to an ejected star gives

$$\frac{G\mu(M_1 + M_2)}{2} \delta \left(\frac{1}{a} \right) = (E_f - E_i) \delta M_{ej} \quad (2)$$

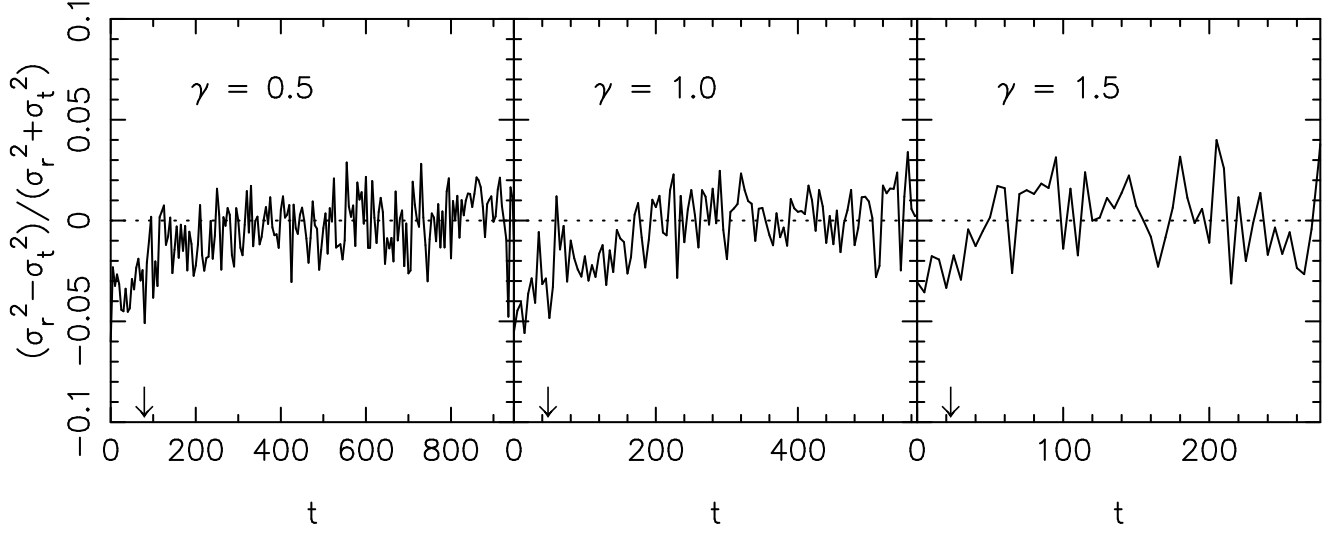


FIG. 4.— Mean velocity anisotropy of the stars in a sphere of radius r'_h around the single black hole, as a function of time after the massive binary was combined into a single particle. Shown are the integrations with $M_2/M_1 = 0.5$. Arrows indicate the time T_{gap} defined in the text (equation 7, Table 1).

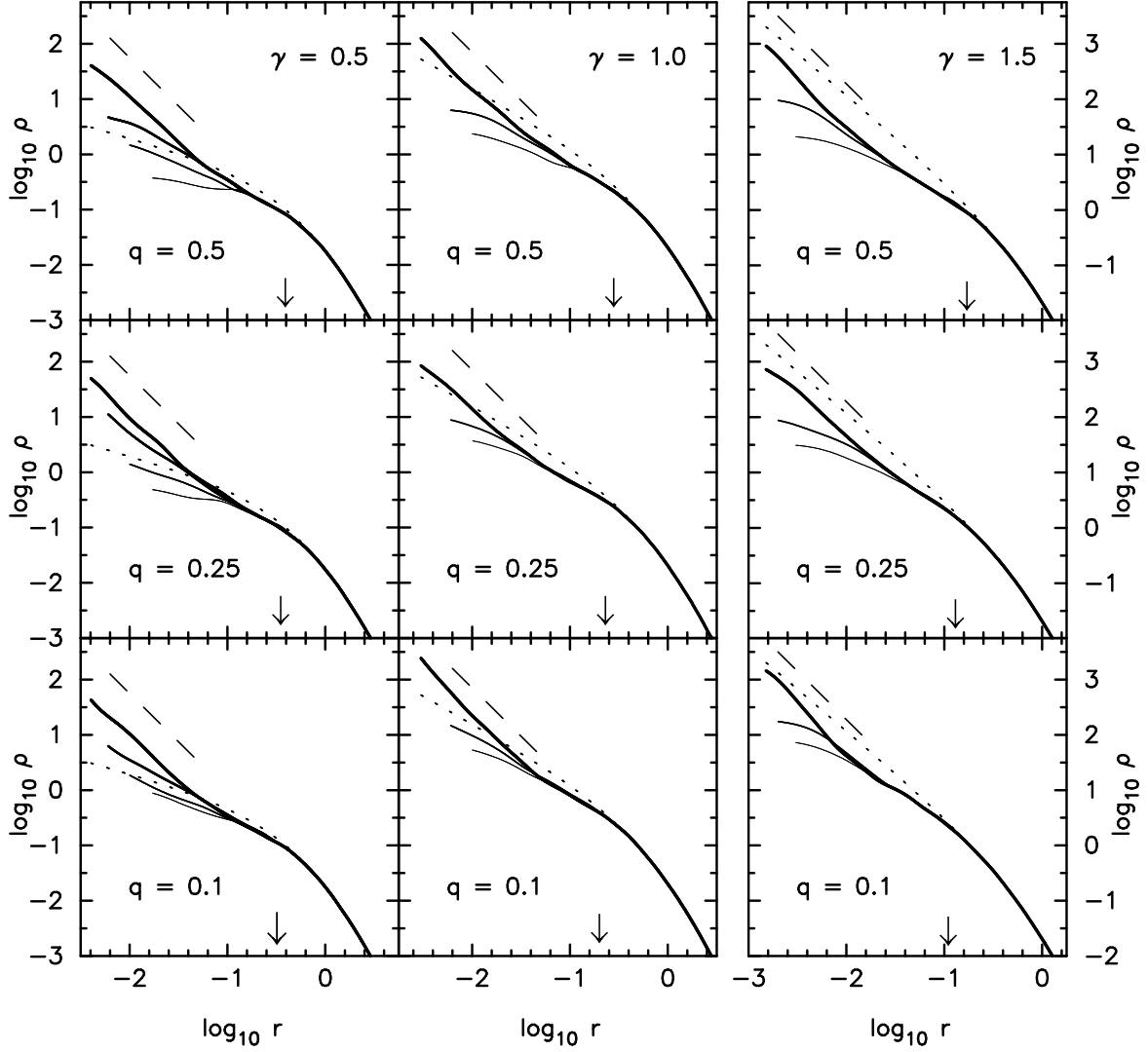


FIG. 5.— Cusp regeneration. Plots show the stellar density profile around the single black hole, at post-coalescence times of approximately $(0, 0.1, 0.5, 1)T_r(r_h)$ ($\gamma = 0.5$), $(0, 0.2, 1)T_r(r_h)$ ($\gamma = 1.0$), and $(0, 0.2, 0.5)T_r(r_h)$ ($\gamma = 1.5$). Dotted lines show the density profiles at the start of the binary integrations, when only one black hole was located at the center. Dashed lines have logarithmic slope of -1.75 . Arrows indicate r'_h , the influence radius of the single black hole just after coalescence of the binary (Table 1).

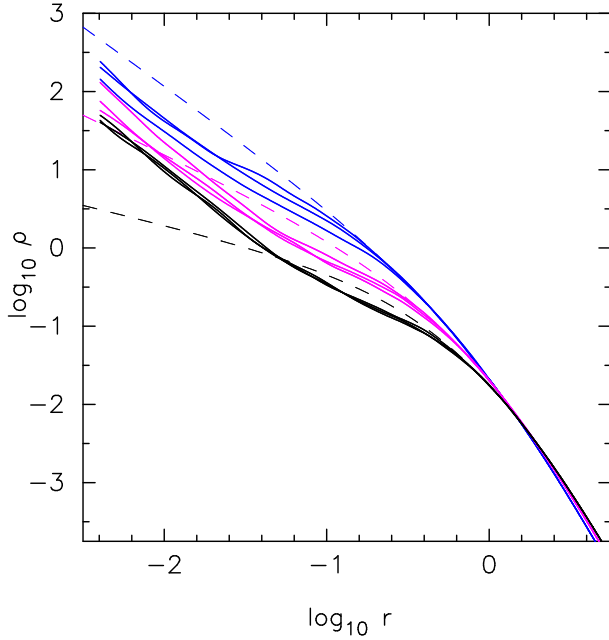


FIG. 6.— Final density profiles after growth of the cusp. Black lines had $\gamma = 0.5$ for the pre-binary initial conditions, red lines had $\gamma = 1.0$, and blue line had $\gamma = 1.5$. Dashed lines show the initial models.

with E_i and E_f the initial and final kinetic energy per unit mass of the ejected star and δM_{ej} its mass; μ is the reduced mass of the binary. This can be written

$$\frac{dM_{ej}}{d \ln(1/a)} = \frac{\mu}{2} \frac{V_{bin}^2}{E_f - E_i} \quad (3)$$

where $V_{bin} = \sqrt{G(M_1 + M_2)/a}$ is the relative velocity between the components of the binary (assuming a circular orbit). Hills (1983) finds from scattering experiments that, for a hard binary in the limit $M_2 \ll M_1$, $E_f - E_i$ for a zero-impact-parameter encounter is $\sim 1.4G\mu/a$. This implies

$$\frac{dM_{ej}}{d \ln(1/a)} \approx 0.36(M_1 + M_2) \quad (4)$$

and the total mass ejected by the binary in hardening from $a \approx a_h$ to a_f is

$$\frac{\Delta M_{ej}}{M_1 + M_2} \approx 0.36 \ln \left(\frac{a_h}{a_f} \right), \quad (5)$$

i.e., the mass ejected in reaching a given degree of hardening a_h/a is proportional to $M_1 + M_2$. Quinlan (1996) used scattering experiments to compute J in the relation

$$\frac{dM_{ej}}{d \ln(1/a)} = J(M_1 + M_2) \quad (6)$$

as a function of M_2/M_1 , assuming a Maxwellian distribution of velocities at infinity. He defined “ejected” stars to be those with final velocities exceeding $\max\{1.5V_0, \sqrt{3}\sigma\}$; here “final” means after the star has moved far from the binary (ignoring any velocity changes that result from the galactic potential), V_0 is the velocity before the encounter, and σ is the velocity dispersion far from the massive binary. Quinlan’s definition is a reasonable one if M_{ej} is to be equated with M_{def} , and Quinlan found that J is nearly independent of M_2/M_1 for a hard binary, decreasing from $J \approx 1$ for $M_2 = M_1$ to $J \approx 0.5$ for

$M_2 = M_1/256$ (his Figure 5). These J -values are consistent with Figure 2.

Expressions like (5) seem counter-intuitive, since they seem to imply an ejected mass that is large even for small M_2 . However for small M_2 , $a_h \propto M_2/M_1$ (equation 1), so for a given a_f , the ejected mass is predicted to scale as $\sim \ln M_2$. The dependence of M_{def} on binary mass ratio is a topic that deserves further study since the central structure of bright elliptical galaxies is expected to reflect the cumulative effect of many minor mergers (Volonteri et al. 2003).

We do observe an additional dependence of M_{def} on both γ and q at given a_h/a (Figure 2). However the definition of a_h is somewhat arbitrary (§2) and we do not pursue that additional dependence here.

The binary preferentially ejects stars on eccentric orbits. The result is an induced anisotropy in the stellar velocity distribution at $r \lesssim r_h$. Figure 3 illustrates this, for the integrations with the most massive secondaries ($M_2/M_1 = 0.5$). The induced anisotropy is mild, similar to what has been observed in other N -body studies (e.g. Milosavljevic & Merritt (2001)).

4. CUSP REGENERATION

When the separation between the two components of the binary had dropped to $a = a_h/5$, the two massive particles were combined into one and placed at the center of mass of the binary. The integrations were then continued until an additional time of roughly $T_r(r'_h)$ had elapsed (Table 1). During this second phase of the integrations, the stellar distribution around the single black hole evolved due to star-star encounters. The initial effect of encounters was to refill the phase space gap created when the binary ejected stars with pericenters $r_p \lesssim a_h$. The refilling time is approximately

$$T_{gap} \approx \frac{a_h}{r_h} T_r(r_h) \approx \frac{1}{4} \frac{q}{(1+q)^2} T_r(r_h) \quad (7)$$

(Merritt & Wang 2005). Table 1 shows that T_{gap} varies between ~ 10 ($\gamma = 1.0, q = 0.1$) and ~ 80 ($\gamma = 0.5, q = 0.5$) in our units, or between $\sim 0.02T_r(r_h)$ and $\sim 0.05T_r(r_h)$. Figure 4 verifies that the initially anisotropic velocity distribution at $r \lesssim r_h$ becomes isotropic in a time of order T_{gap} . In luminous galaxies, even T_{gap} can exceed a galaxy lifetime (Merritt & Wang 2005), and such galaxies will experience a greatly reduced rate of interaction of stars with the black hole compared to galaxies with a full loss cone.

On the longer time scale of $\sim T_r(r_h)$, energy exchange between stars modifies their radial distribution, eventually reaching the zero-flux Bahcall-Wolf (1976) solution $\rho \sim r^{-7/4}$. This is shown in Figure 5 for the $\gamma = 0.4$ and $\gamma = 1$ models. (Results for $\gamma = 1.5$ are shown in Figures 6 and 7 and are discussed separately below.) The new cusp attains the $\rho \sim r^{-7/4}$ form inside of $\sim 0.2r'_h$. In all of the integrations, the logarithmic slope of the final cusp is steeper than that of the initial (pre-binary) galaxy at radii $r \lesssim 0.5r'_h$, although the final density remains below the initial density at $r \approx r'_h$.

Figure 6 shows the final density profiles for all seven models. There is remarkably little dependence of the final result on the mass ratio of the binary. The reason can be seen by comparing Figures 1 and 6: while the different mass ratios do yield different density profiles at the end of the binary phase, most of these differences are at $r \lesssim 0.3r_h$, and this region is efficiently refilled by the new cusp.

The final density profiles in Figure 6 can be well approxi-

mated as broken power laws at radii $r \lesssim r_h$:

$$\begin{aligned} \rho(r) &= \rho(r_0) \left(\frac{r}{r_0} \right)^{-7/4}, \quad r \leq r_0, \\ &= \rho(r_0) \left(\frac{r}{r_0} \right)^{-1}, \quad r_0 < r \lesssim r_h. \end{aligned} \quad (8)$$

The “break” radius r_0 is $\sim 0.15r'_h$ in the models with initial cusp slope $\gamma = 0.5$, $\sim 0.20r'_h$ for $\gamma = 1.0$, and $\sim 0.25r'_h$ for $\gamma = 1.5$. In this approximation to $\rho(r)$, the mass in the cusp, $M_{cusp} \equiv M(r \leq r_0)$, is given by

$$M_{cusp} = \frac{2M_\bullet}{1 + 0.75 \left[(r_h/r_0)^2 - 1 \right]}. \quad (9)$$

Thus $M_{cusp}/M_\bullet \approx 0.03$ ($\gamma = 0.5$), ~ 0.12 ($\gamma = 1.0$), and ~ 0.16 ($\gamma = 1.5$), confirming that M_{cusp} is small compared with M_\bullet . One consequence is that r''_h , the influence radius at the final time step, differs only slightly from r'_h , the influence radius at the end of the binary phase (Table 1).

Finally, we consider how much time is required to regrow the cusps. As noted above, all of the post-binary integrations were carried out until an elapsed time of $\sim T_r(r'_h)$, and this was also roughly the time required for the cusp to reach its steady-state form. However the cusp extends only to a radius of $\sim 0.2r'_h$, and a more relevant estimate of the relaxation time is probably $T_r(0.2r'_h)$. Estimates of this time are given in Table 1. The time to fully grow the cusp is approximately 2–3 times the relaxation time at $0.2r'_h$. As Figure 5 shows, considerable regeneration takes place even in a much shorter time, hence we might predict the presence of steep central profiles even in galaxies substantially younger than either $T_r(r_h)$ or $(2-3)T_r(0.2r_h)$. We return to this issue below.

5. IMPLICATIONS

5.1. Cusp Regeneration in Local Group Galaxies

The relaxation time in the Milky Way nucleus is less than 10^{10} yr and a number of authors have suggested that the stellar cluster around the supermassive black hole might be collisionally relaxed (Alexander 1999; Genzel et al. 2003). The stellar mass density, based on number counts that extend down to ~ 0.005 pc, is

$$\rho(r) \approx 1.2 \times 10^6 M_\odot \text{pc}^{-3} \left(\frac{r}{0.38 \text{pc}} \right)^{-\alpha} \quad (10)$$

(Genzel et al. 2003), with $\alpha \approx 2.0$ at $r \geq 0.38$ pc and $\alpha \approx 1.4$ at $r < 0.38$ pc. The black hole mass is $3.7 \pm 0.2 \times 10^6 M_\odot$ (Ghez et al. 2005). The implied influence radius, defined as the radius containing a mass in stars that is twice the black hole mass, is $r_h \approx 88'' \approx 3.4$ pc.

We used equation (10) and the measured value of M_\bullet to compute the stellar velocity dispersion profile in the Milky Way nucleus, assuming a spherical velocity ellipsoid. The relaxation time T_r was then calculated as in the N -body models, i.e.

$$T_r(r) = \frac{0.338\sigma(r)^3}{\rho(r)m_\star G^2 \ln \Lambda} \quad (11a)$$

$$\approx 1.69 \times 10^9 \text{yr} \times \quad (11b)$$

$$\left(\frac{\sigma(r)}{100 \text{ km s}^{-1}} \right)^3 \left(\frac{\rho(r)}{10^6 M_\odot} \right)^{-1} \left(\frac{m_\star}{0.7 M_\odot} \right)^{-1} \left(\frac{\ln \Lambda}{15} \right)^{-1} \quad (11c)$$

with $m_\star = 0.7 M_\odot$ and $\Lambda = \sigma^2(r_h)r_h/2Gm_\star$. The relaxation time at $r = r_h$ was found to be 5.4×10^{10} yr, dropping to $\sim 6 \times 10^9$ yr at $0.2r_h$ and $\sim 3.5 \times 10^9$ yr at $\sim 0.1r_h$; at smaller radii, T_r increases very slowly with decreasing r .

As noted above, cusp regeneration in the N -body models required a time of $\sim 1T_r(r_h)$, or $\sim 2-3T_r(0.2r_h)$. However these two timescales are substantially different in the Milky Way, suggesting that the structure of the Milky Way nucleus differs in some respect from that of the N -body models in the region $0.2r_h \lesssim r \lesssim r_h$.

Figure 7 makes the comparison. We show the evolution of $\rho(r)$ and $\Sigma(R)$ (the latter is the projected density) in the post-binary integration with parameters ($\gamma = 1.5, q = 0.5$); the right-hand frame also shows the measured surface density of stars at the Galactic center, from the number counts of Genzel et al. (2003), with arbitrary vertical normalization. The N -body model successfully reproduces the slope of the observed stellar cusp at late times, but the N -body profile is less steep than the observed counts at $r \gtrsim 0.2r_h$, i.e., outside of the cusp. In the Milky Way, an approximately power-law dependence of ρ on r extends well beyond r_h , while the N -body models exhibit a shallower slope at these radii. Better correspondence between N -body model and data could presumably have been achieved by modifying the initial model, or by repeating the integrations with smaller M_\bullet (which would have mandated a larger N in order to resolve the smaller cusp); the unphysically large value of M_\bullet adopted here ($M_\bullet = 0.015 M_{\text{gal}}$) implies an influence radius that is comparable to the Dehnen-model scale length.

In light of these ambiguities, it is reasonable to fix the physical unit of time by comparing the N -body model to the Milky Way at $\sim 0.2r_h$; this is roughly the outer radius of the cusp, and Figure 7 shows that the model fits the data well out to this radius. We find that $T_r(0.2r_h) \approx 160$ in N -body units, while in the Milky Way, $T_r(0.2r_h) \approx 6 \times 10^9$ yr. The integration time of 300 in Figure 7 then corresponds to a physical time of $\sim 1.1 \times 10^{10}$ yr. In fact, the N -body cusp attains nearly its final form by a time of ~ 200 , or $\sim 8 \times 10^9$ yr. We conclude that the distribution of stars near the Milky Way black hole is consistent with a merger having occurred at a time $\gtrsim 8$ Gyr in the past.

In fact, the probability is $\sim 68\%$ that a galaxy with a dark-matter halo as large as that of the Milky Way has experienced a major merger (mass ratio of at least 4 : 1) since a redshift of $z = 2$, i.e., in the last ~ 10 Gyr (Merritt et al. 2002). If this occurred, our results suggest the interesting possibility that the Milky Way cusp may still be evolving toward its steady-state form. Evidence for this might be sought in the form of a flattening the density profile at very small radii, $r \lesssim 0.1r_h \approx 10''$.

The stellar density near the center of M32 is

$$\rho(r) \approx 2.2 \times 10^5 M_\odot \text{pc}^{-3} \left(\frac{r}{1 \text{pc}} \right)^{-\alpha}, \quad \alpha \approx 1.5 \quad (12)$$

(Lauer et al. 1998), very similar to that of the Milky Way. Unfortunately the estimation of M_\bullet in M32 suffers from the degeneracy inherent in orbital modelling of axisymmetric systems and the black hole mass could lie anywhere in the range $1.5 \times 10^6 M_\odot \lesssim M_\bullet \lesssim 5 \times 10^6 M_\odot$ with equal likelihood (Valluri, Merritt & Emsellem 2004). Applying the $M_\bullet - \sigma$ relation (Ferrarese & Merritt 2000) gives $M_\bullet \approx 2.0 \times 10^6 M_\odot$ which we adopt here. The black hole influence radius becomes ~ 1.7 pc $\approx 0.5''$ and $T_r(r_h) \approx 2.2 \times 10^{10}$ yr. This is

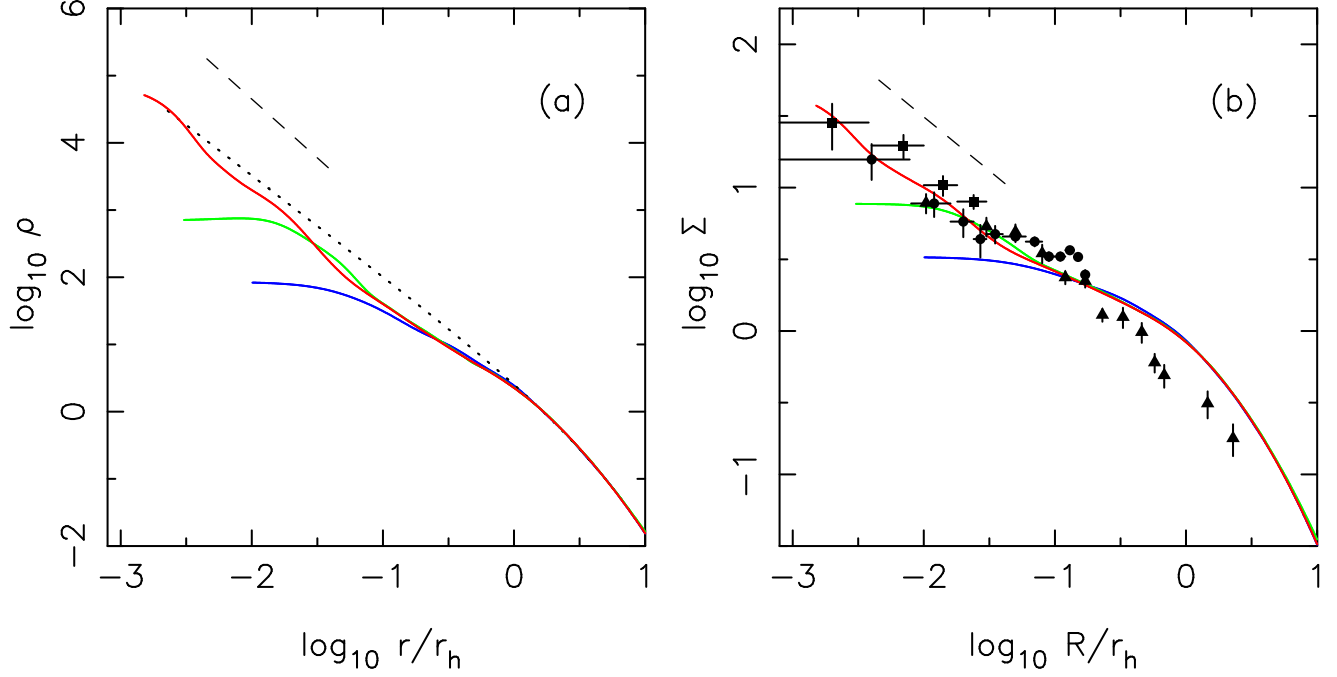


FIG. 7.— Evolution of the spatial (a) and projected (b) density profiles in the simulation that most closely resembles the Milky Way nucleus. The initial model (dotted line) had a $\rho \sim r^{-1.5}$ density cusp and a central black hole of mass $M_1 = 0.01$, in units where the total stellar mass of the model is 1. Blue (lower) line shows the density after infall and capture of a second black hole of mass $M_2 = 0.1M_1$. Green and red lines show the evolving density at times (40, 100) after coalescence; based on the discussion in the text, the corresponding physical times are roughly $(3, 8) \times 10^9$ yr. Symbols in (b) show the observed surface density of stars near the Galactic Center, from Genzel et al. (2003); see Figure 7 from that paper for symbol definitions. The vertical normalization of the symbols was set by eye in order to give a good match to the N -body data at $R \lesssim 0.2r_h$. Dashed lines have logarithmic slopes of -1.75 (a) and -0.75 (b).

somewhat smaller than the estimate of $T_r(r_h)$ in the Galactic nucleus, suggesting that a collisional cusp could easily have been regenerated in M32. However, the cusp should only extend outward to $\sim 0.2r_h \approx 0.1''$ at the distance of M32, barely resolvable even with HST. Depending on the exact value of M_\bullet , the collisional cusp in M32 may or may not have been resolved.

Both the mass of the black hole in M31, and the dynamical state of its nucleus, are less certain than in the Milky Way and M32 due to M31's complex morphology. However most estimates of the relaxation time at the center of P2, the nuclear component believed to contain the black hole, are of order 10^{11} yr (e.g. Lauer et al. 1998). M33 has a very short central relaxation time but no dynamical signature of a black hole (Valluri et al. 2005).

5.2. Cusp Regeneration in Galaxies Beyond the Local Group

Which galaxies beyond the Local Group should contain Bahcall-Wolf cusps? Figure 8 shows estimates of $T_r(r_h)$ in the sample of early-type galaxies modelled by Wang & Merritt (2004); these are a subset of the Magorrian et al. (1998) galaxies. In this plot, filled symbols denote galaxies observed with angular resolution $\theta_{obs} < \theta_{r_h}$, and the size of the symbol is proportional to $\log(\theta_{r_h}/\theta_{obs})$. (In galaxies where r_h is not resolved, we note that the estimates of T_r are particularly uncertain, since they depend on an inward extrapolation of luminosity profiles measured at $r > r_h$.)

Figure 8 reveals that the brightest spheroids, $M_V \lesssim -20$, have central relaxation times that always greatly exceed 10^{10} yr. In these galaxies, a low-density core created by a binary supermassive black hole would persist for the age of the universe. However $T_r(r_h)$ drops with decreasing luminos-

ity, falling below 10^{10} yr for $M_V \gtrsim -18$. The Milky Way bulge falls on the relation defined by the more distant galaxies, which is reassuring given the uncertainties in its luminosity. (We adopted a bulge blue absolute magnitude of $M_B = -17.6$ from Marconi & Hunt (2003) and assumed $M_V = M_B - 0.9$.) However M32 appears to be shifted from the relation defined by the other galaxies, as if it is the dense core of a once much brighter galaxy. This possibility has often been raised in the past (King 1962; Faber 1973; Nieto & Prugniel 1987).

Figure 8, combined with the arguments in §5.1, suggests that spheroids fainter than $M_V \approx -18.5$ are dynamically old enough to contain Bahcall-Wolf cusps.

However outside of the Local Group, Figure 8 also suggests that such cusps are unlikely to be resolved. We can check this prediction by relating the angular size of the cusp to black hole mass via the $M_\bullet - \sigma$ relation, $M_8 \approx 1.66\sigma_{200}^{4.86}$ (Ferrarese & Ford 2005), with $M_8 \equiv M_\bullet/10^8 M_\odot$ and $\sigma_{200} \equiv \sigma/200 \text{ km s}^{-1}$, and (temporarily) redefining r_h as $GM_\bullet/\sigma^2 \approx 11.2M_8\sigma_{200}^{-2} \text{ pc}$. Then

$$r_h \approx 2.76M_8^{0.59} \text{ pc}. \quad (13)$$

Taking for the outer radius of the cusp $r_0 \approx 0.2r_h$ (equation 8), its angular size becomes

$$\theta_0 \approx 0.57'' M_8^{0.59} D_{Mpc}^{-1} \quad (14)$$

with D_{Mpc} the distance to the galaxy in Mpc. Thus, at the distance of the Virgo cluster, $\theta_0 > 0.1''$ implies $M_\bullet \gtrsim 6 \times 10^8 M_\odot$; however such massive black holes would almost certainly sit in galaxies with central relaxation times longer than 10^{10} yr (Figure 8) and a cusp would not have formed. If we assume that black holes like the ones in the Milky Way and M32 (i.e.

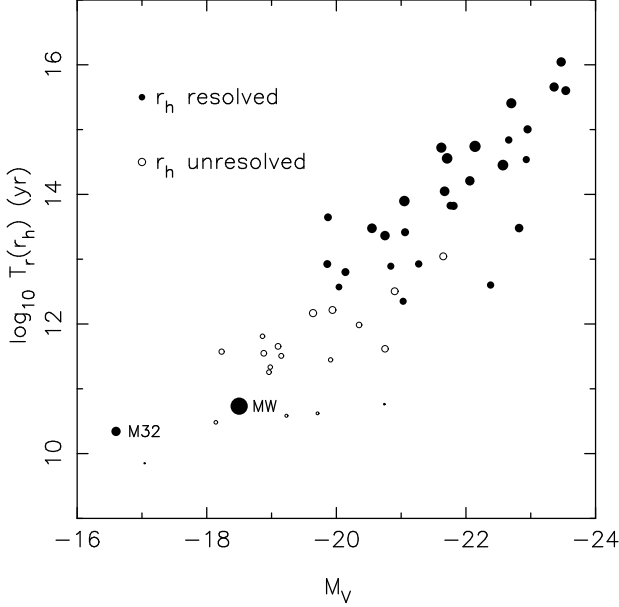


FIG. 8.— Estimates of the relaxation time at the black hole’s influence radius, r_h , in the sample of early-type galaxies modelled by Wang & Merritt (2004). Black hole masses were computed from the $M_\bullet - \sigma$ relation (Merritt & Ferrarese 2001), except in the case of the Milky Way, for which $M_\bullet = 3.7 \times 10^6 M_\odot$ was assumed (Ghez et al. 2005). The stellar mass was set equal to $0.7 M_\odot$ when computing T_r . Horizontal axis is absolute visual magnitude of the galaxy or, in the case of the Milky Way, the stellar bulge. The size of the symbols is proportional to $\log_{10}(\theta_{r_h}/\theta_{obs})$, where θ_{r_h} is the angular size of the black hole’s influence radius and θ_{obs} is the observational resolution. Filled symbols have $\theta_{r_h} > \theta_{obs}$ (r_h resolved) and open circles have $\theta_{r_h} < \theta_{obs}$ (r_h unresolved). Values of $T_r(r_h)$ in the unresolved galaxies should be considered approximate since the luminosity profiles in these galaxies are not well known at $r < r_h$.

$M_\bullet \approx 3 \times 10^6 M_\odot$) are the most massive to be associated with collisionally-relaxed nuclei, then the associated cusps could be resolved to a distance of ~ 0.7 Mpc, roughly the distance to M32 – consistent with the statement made above that the cusp in M32 is only barely resolved. Hence, collisional cusps are unlikely to be observed in galaxies beyond the Local Group.

Unresolved density cusps might appear as pointlike nuclei, particularly in dE galaxies which have low central surface brightnesses. Pointlike nuclei are in fact nearly ubiquitous in elliptical galaxies as faint as $M_V \approx -18$, disappearing for $M_V \gtrsim -13$ (van den Bergh 1986). Luminosities of the nuclei are observed to average ~ 0.003 times that of their host galaxies, albeit with considerable scatter (Coté et al. 2005). As shown in §4, Bahcall-Wolf cusps entrain a mass of order $0.1 M_\bullet$. If the ratio of black hole mass to stellar mass that characterizes bright galaxies, $M_\bullet/M_{gal} \approx 0.0013$ (Merritt & Ferrarese 2001), also holds for dE galaxies, the luminosity associated with the cusps would be only $\sim 10^{-4} L_{gal}$, too small to explain the majority of the observed nuclei. On the other hand, essentially nothing is known about the masses (or even the existence) of black holes in spheroids fainter than $M_V = -18$ (with the exception of M32, probably a special case) and it is possible that $M_\bullet \gtrsim 10^{-3} M_{gal}$ in these galaxies. It is intriguing to speculate that the disappearance of pointlike nuclei in dE galaxies fainter than $M_V \approx -13$ might signal the disappearance of the black holes.

We note that the nuclear cusps of the Milky Way and M32 extend approximately as power laws out to radii far beyond r_h . Even these more extended cusps would be unresolved beyond

the Local Group and might contain enough light to explain the pointlike nuclei. The existence of these extended power-law cusps – which presumably have little to do with the presence of the black holes – suggests that other mechanisms, e.g. star formation triggered by gas infall, might be as effective as stellar dynamics at re-generating cusps.

The black holes in the Milky Way and M32 are among the smallest with dynamically-determined masses (Ferrarese & Ford 2005). If smaller black holes do not exist, Figure 8 suggests that Bahcall-Wolf cusps might be present only in a small subset of spheroids containing black holes with masses $10^6 M_\odot \lesssim M_\bullet \lesssim 3 \times 10^6 M_\odot$. However it has been argued that some late-type spirals host AGN with black hole masses as low as $\sim 10^4 M_\odot$ (Ho 2004). If so, Figure 8 suggests that Bahcall-Wolf cusps would be present around these black holes.

The presence of cores, or “mass deficits,” at the centers of bright elliptical galaxies has been taken as evidence of past merger events (Milosavljevic et al. 2002; Ravindranath, Ho & Filippenko 2002; Graham 2004). Mass deficits are observed to disappear in galaxies fainter than $M_V \approx -19.5$ (Milosavljevic et al. 2002). Could this be due to cusp regeneration? Figure 8 suggests an alternative explanation. Galaxies fainter than $M_V = -19.5$ are mostly unresolved on scales of r_h , which is also the approximate size of a core created by a binary supermassive black hole. The lack of mass deficits in galaxies with $M_V \gtrsim -19.5$ probably just reflects a failure to resolve the cores in these galaxies.

5.3. Black Hole Feeding Rates

The low-luminosity galaxies most likely to harbor Bahcall-Wolf cusps (Figure 8) are the same galaxies that would dominate the overall rate of stellar tidal disruptions, assuming of course that they contain black holes (Wang & Merritt 2004). Published estimates of \dot{N} , the rate of stellar disruptions, in such low-luminosity galaxies (Syer & Ulmer 1999; Magorrian & Tremaine 1999; Wang & Merritt 2004) have almost always been based on an inward extrapolation of luminosity profiles measured at $r > r_h$. In principle, knowing that $\rho(r)$ has the Bahcall-Wolf form near the black hole should allow a more accurate estimate of \dot{N} in the low-luminosity galaxies that dominate the overall flaring rate.

Here we show that the presence of a Bahcall-Wolf cusp implies a lower limit on \dot{N} , of order 10^{-4} yr^{-1} . The stellar density in the cusp is

$$\rho(r) \approx \rho(r_0) \left(\frac{r}{r_0} \right)^{-7/4} \quad (15)$$

(equation 8), with $r_0 = \alpha r_h$, $\alpha \approx 0.2$. We can write $\rho(r_0) = K M_\bullet / r_h^3$, where the constant K depends on the form of $\rho(r)$ at $r > r_0$; assuming a $\rho \sim r^{-2}$ power law for $r > r_0$, as in the Milky Way and many other low-luminosity spheroids, we find $K \approx 4.0$. The rate at which stars in the cusp are fed to the black hole is approximately

$$\dot{N}_{cusp} \approx \frac{4\pi}{m_\star} \int_0^{\omega r_h} \frac{\rho}{T_r \ln(2/\theta_{lc})} r^2 dr \quad (16)$$

(Lightman & Shapiro 1977; Syer & Ulmer 1999). Here $\theta_{lc} \approx \sqrt{r_t/r}$ is the angular size of the loss cone at radius r and r_t is the tidal disruption radius, $r_t \approx (M_\bullet/m_\star)^{1/3} r_\star$. This expression assumes that the feeding rate is limited by diffusion, i.e. that the loss cone is “empty”; an equivalent statement

is that r_{crit} , the radius above which a star can scatter in and out of the loss cone in one orbital period, is greater than αr_h . In the case of the Milky Way black hole, it can be shown that $0.2r_h < r_{crit} < r_h$. Taking the slowly-varying logarithmic terms out of the integral, we find a feeding rate for stars in the cusp:

$$\dot{N}_{cusp} \approx 1.6 \frac{\ln \Lambda}{\ln(2/\theta_{lc})} \left(\frac{GM_\bullet}{r_h^3} \right)^{1/2}. \quad (17)$$

Evaluating θ_{lc} at $r = \alpha r_h$ and setting $\ln \Lambda = 15$, this becomes

$$\dot{N}_{cusp} \approx 7 \times 10^{-5} \text{yr}^{-1} M_{\bullet, MW}^{1/2} r_{h, MW}^{-3/2} \quad (18)$$

where $M_{\bullet, MW}$ and $r_{h, MW}$ are in units of the values quoted above for the Milky Way. Thus, the flaring rate due to stars in the Milky Way cusp is $\sim 10^{-4} \text{yr}^{-1}$. This is of course a lower limit on the total \dot{N} since it ignores the contribution from stars outside the cusp, at $r > \alpha r_0 \approx 0.7 \text{ pc}$. In fainter spheroids, the $M_\bullet - \sigma$ relation, combined with equation (18), implies $\dot{N} \propto M_\bullet^{-0.4}$ and hence even higher flaring rates.

The Bahcall-Wolf solution will break down at radii where the physical collision time is shorter than the diffusion time $\ln(2/\theta_{lc})T_r$. Adopting the standard expression for the collision time,

$$T_{coll} = [16\sqrt{\pi}n\sigma r_\star^2(1 + \Theta)]^{-1} \quad (19)$$

with $\Theta \equiv Gm_\star/(2\sigma^2 r_\star)$ and n the number density of stars, we find that physical collisions begin to affect the stellar distribution at $r \lesssim 0.08 \text{ pc} \lesssim 0.023r_h$ for Solar-type stars in the Galactic nucleus.

5.4. Gravitational Lensing

The central parts of galaxies can act as strong gravitational lenses; the lack of a “core” image in observed lens systems implies a lower limit on the stellar density of the lensing galaxy within the central $\sim 10^2 \text{ pc}$ (Rusin & Ma 2001; Keeton 2003). Broken power-law density profiles like those in equation (8) have been used to model lensing galaxies (Muñoz et al. 2001; Bowman et al. 2004), although the break radii in these studies were chosen to be much larger than the value $r_0 \approx 0.2r_h$ that describes the Bahcall-Wolf cusps (Figure 6). However the presence or absence of the cusps should

have little effect on the lensing properties of galaxies, because the mass contained within the cusp is small compared with M_\bullet , and because even the supermassive black holes contribute only slightly to the lensing signal (Rusin et al. 2005). The low-luminosity galaxies that are likely to contain cusps (Figure 8) are also unlikely to act as lenses.

5.5. Dark Matter

The distribution of *dark matter* on sub-parsec scales near the center of the Milky Way and other galaxies is relevant to the so-called “indirect detection” problem, in which inferences are drawn about the properties of particle dark matter based on measurements of its self-annihilation by-products (Bertone & Merritt 2005). A recent detection of TeV radiation from the Galactic center by the HESS consortium (Aharonian et al. 2004) is consistent with a particle annihilation signal, but only if the dark matter density in the inner few parsecs is much higher than predicted by an inward extrapolation of the standard, Λ CDM halo models (Hooper et al. 2004). One possibility is that the dark matter forms a steep “spike” around the black hole (Gondolo & Silk 1999). Particle dark matter would not spontaneously form a Bahcall-Wolf cusp since its relaxation time is extremely long. However, once a cusp forms in the *stars*, scattering of dark matter particles off of stars would redistribute the dark matter in phase space on a time scale of order $T_r(r_h)$, the star-star relaxation time (Merritt 2004). The ultimate result is a $\rho \sim r^{-3/2}$ density cusp in the dark matter (Gnedin & Primack 2004), but with possibly low normalization, particularly if the dark matter distribution was previously modified by a binary black hole (Merritt et al. 2002). The N -body techniques applied here would be an effective way to address this problem.

P. Coté, L. Ferrarese, C. Keeton, S. Portegies Zwart, A. Robinson, D. Rusin and the referee, H. Baumgardt, made comments and suggestions that improved this paper. R. Genzel kindly provided the Galactic center number count data that are reproduced in Figure 7. This work was supported by grants AST-0071099, AST-0206031, AST-0420920 and AST-0437519 from the NSF, grant NNG04GJ48G from NASA, and grant HST-AR-09519.01-A from STScI.

REFERENCES

- Aarseth, S. J. 1999, *PASP*, 111, 1333
Aarseth, S. J. 2003, *Ap&SS*, 285, 367
Aharonian, F., et al. 2004, *A&A*, 425, L1
Alexander, T. 1999, *ApJ*, 527, 835
Bahcall, J. N. & Wolf, R. A. 1976, *ApJ*, 209, 214
Baumgardt, H., Makino, J., & Ebisuzaki, T. 2004, *ApJ*, 613, 1133
Baumgardt, H., Makino, J., & Ebisuzaki, T. 2004, *ApJ*, 613, 1143
Berczik, P., Merritt, D. & Spurzem, R. 2005, *astro-ph/0507260*
Bertone, G., & Merritt, D. 2005, *Modern Physics Letters A*, 20, 1021
Bowman, J. D., Hewitt, J. N., & Kiger, J. R. 2004, *ApJ*, 617, 81
Boylan-Kolchin, M., Ma, C.-P., & Quataert, E. 2004, *ApJ*, 613, L37
Cohn, H., & Kulsrud, R. M. 1978, *ApJ*, 226, 1087
Coté, P., Piatek, S., Ferrarese, L., P., Jordán, A., Merritt, D., Peng, E. W., Hasegan, M., Blakeslee, J. P., Mei, S., West, M. J., Milosavljević, M., & Tonry, J. L. 2005, submitted to *The Astrophysical Journal*.
Dehnen, W. 1993, *MNRAS*, 265, 250
Faber, S. M. 1973, *AJ*, 179, 423
Ferrarese, L., Coté, P., Jordán, A., Peng, E. W., Blakeslee, J. P., Piatek, S., Mei, S., Merritt, D., Milosavljević, M., Tonry, J. L., & West, M. J. 2005, submitted to *The Astrophysical Journal*.
Ferrarese, L., & Ford, H. 2005, *Space Science Reviews*, 116, 523
Ferrarese, L., & Merritt, D. 2000, *ApJ*, 539, L9
Frank, J., & Rees, M. J. 1976, *MNRAS*, 176, 633
Gebhardt, K. et al. 1996, *AJ*, 112, 105
Genzel, R., Schödel, R., Ott, T., Eisenhauer, F., Hofmann, R., Lehnert, M., Eckart, A., Alexander, T., Sternberg, A., Lenzen, R., ClA@net, Y., Lacombe, F., Rouan, D., Renzini, A., & Tacconi-Garman, L. E. *ApJ*, 594, 812
Ghez, A. M., Salim, S., Hornstein, S. D., Tanner, A., Lu, J. R., Morris, M., Becklin, E. E., & Duchêne, G. 2005, *ApJ*, 620, 744
Gnedin, O. Y., & Primack, J. R. 2004, *Physical Review Letters*, 93, 061302
Gondolo, P., & Silk, J. 1999, *Physical Review Letters*, 83, 1719
Graham, A. W. 2004, *ApJ*, 613, L33
Hills, J. G. 1983, *AJ*, 88, 1269
Ho, L. 2004, in *Carnegie Observatories Astrophysics Series, Vol. 1: Coevolution of Black Holes and Galaxies*, ed. L. C. Ho (Cambridge: Cambridge Univ. Press), p. 292
Hooper, D., de la Calle Perez, I., Silk, J., Ferrer, F., & Sarkar, S. 2004, *Journal of Cosmology and Astro-Particle Physics*, 9, 2
Keeton, C. R. 2003, *ApJ*, 582, 17
King, I. R. 1962, *AJ*, 67, 471
Lauer, T. et al. 1998, *AJ*, 116, 2263
Lightman, A. P. & Shapiro, S. L. 1977, *ApJ*, 211, 244
Magorrian, J. et al. 1998, *AJ*, 115, 2285

- Magorrian, J. & Tremaine, S. 1999, *MNRAS*, 309, 447
- Marconi, A. & Hunt, L. K. 2003, *ApJ*, 589, L21
- Merritt, D. 2004a, "Single and Binary Black Holes and their Influence on Nuclear Structure," in *Carnegie Observatories Astrophysics Series, Vol. 1: Coevolution of Black Holes and Galaxies*, ed. L. C. Ho (Cambridge: Cambridge Univ. Press)
- Merritt, D. 2004, *Physical Review Letters*, 92, 201304
- Merritt, D. & Ferrarese, L. 2001, *MNRAS*, 320, L30
- Merritt, D. & Ferrarese, L. 2001, in *ASP Conf. Ser. 249, The Central Kiloparsec of Starbursts and AGN: The La Palma Connection*, ed. J. H. Knapen et al. (San Francisco: ASP), 335
- Merritt, D., Mikkola, S. & Szell, A. 2006, in preparation
- Merritt, D. & Milosavljevic, M. 2005, "Massive Black Hole Binary Evolution," *Living Reviews in Relativity*
- Merritt, D., Milosavljevic, M., Favata, M., Hughes, S. A. & Holz, D.E. 2004, *ApJ*, 607, L9
- Merritt, D., Milosavljevic, M., Verde, L. & Jimenez, R. 2002, *Phys. Rev. Lett.*, 88, 191301
- Merritt, D. & Tremblay, B. 1994, *AJ*, 108, 514
- Merritt, D. & Wang, J. 2005, *ApJ*, 621, L101
- Mikkola, S., & Aarseth, S. J. 1990, *Celestial Mechanics and Dynamical Astronomy*, 47, 375
- Mikkola, S., & Aarseth, S. J. 1993, *Celestial Mechanics and Dynamical Astronomy*, 57, 439
- Mikkola, S., & Valtonen, M. J. 1992, *MNRAS*, 259, 115
- Milosavljevic, M. & Merritt, D. 2001, *ApJ*, 563, 34
- Milosavljevic, M. & Merritt, D. 2003, *ApJ*, 596, 860
- Milosavljevic, M., Merritt, D., Rest, A., & van den Bosch, F. C. 2002, *MNRAS*, 331, 51
- Muñoz, J. A., Kochanek, C. S., & Keeton, C. R. 2001, *ApJ*, 558, 657
- Murphy, B. W., Cohn, H. N. & Durisen, R. H. 1991, *ApJ*, 370, 60
- Nakano, T. & Makino, J. 1999a, *ApJ*, 510, 155
- Nakano, T. & Makino, J. 1999b, *ApJ*, 525, L77
- Nieto, J.-L. & Prugniel, P. 1987, *â*, 186, 30
- Preto, M., Merritt, D. & Spurzem, R. 2004, *ApJ*, 613, L109
- Quinlan, G. D. 1996, *New Astron.* 1, 35
- Quinlan, G. D. 1997, *New Astron.* 2, 533
- Ravindranath, S., Ho, L. C. & Filippenko, A. V. 2002, *ApJ*, 566, 801
- Rest, A. et al. 2001, *AJ*, 121, 2431
- Rusin, D., Keeton, C. R., & Winn, J. N. 2005, *ApJ*, 627, L9
- Rusin, D., & Ma, C.-P. 2001, *ApJ*, 549, L33
- Saslaw, W. C., Valtonen, M. J., & Aarseth, S. J. 1974, *ApJ*, 190, 253
- Spitzer, L. 1987, "Dynamical Evolution of Globular Clusters" (Princeton: Princeton University Press)
- Syer, D. & Ulmer, A. 1999, *MNRAS*, 306, 35
- Szell, A., Merritt, D. & Mikkola, S. 2005, in *Nonlinear Dynamics in Astronomy & Physics*, ed. S. T. Gottesman, J.-R. Buchler & M. E. Mahon, *Ann. N. Y. Acad. Sci.* 1045, 225
- Valluri, M., Ferrarese, L., Merritt, D. & Joseph, C. L. 2005, *ApJ*, 628, 137
- Valluri, M., Merritt, D., & Emsellem, E. 2004, *ApJ*, 602, 66
- van den Bergh, S. 1986, *AJ*, 91, 271
- Volonteri, M., Madau, P., & Haardt, F. 2003, *ApJ*, 593, 661
- Wang, J. & Merritt, D. 2004, *ApJ*, 600, 149
- Young, P. J. 1977, *ApJ*, 215, 36
- Yu, Q. 2002, *MNRAS*, 331, 935